

Optical Engineering

OpticalEngineering.SPIEDigitalLibrary.org

Three-dimensional reflection screens fabricated by holographic wavefront printer

Ryutaro Oi
Ping-Yen Chou
Boaz Jessie Jackin
Koki Wakunami
Yasuyuki Ichihashi
Makoto Okui
Yi-Pai Huang
Kenji Yamamoto

SPIE.

Ryutaro Oi, Ping-Yen Chou, Boaz Jessie Jackin, Koki Wakunami, Yasuyuki Ichihashi, Makoto Okui, Yi-Pai Huang, Kenji Yamamoto, "Three-dimensional reflection screens fabricated by holographic wavefront printer," *Opt. Eng.* **57**(6), 061605 (2018), doi: 10.1117/1.OE.57.6.061605.

Three-dimensional reflection screens fabricated by holographic wavefront printer

Ryutaro Oi,^{a,*} Ping-Yen Chou,^b Boaz Jessie Jackin,^a Koki Wakunami,^a Yasuyuki Ichihashi,^a Makoto Okui,^a Yi-Pai Huang,^b and Kenji Yamamoto^a

^aNational Institute of Information and Communications Technology, Electromagnetic Research Institute, Electromagnetic Applications Laboratory, Koganei, Tokyo, Japan

^bNational Chiao Tung University, Department of Photonics and Institute of Electro-Optical Engineering, Hsinchu, Taiwan

Abstract. Several wavefront printers have been recently proposed. Since the printers can record an arbitrary computer-generated wavefront, they are expected to be useful for fabricating complex mirror arrays used in front projection 3-D screens without using real existing optics. We prototyped two transparent reflective screens using our hologram printer in experiments. These screens could compensate for a spherically distorted reference wave caused by a short projection distance to obtain an ideal reference wave. Owing to the use of the wavefront-printed screen, the 3-D display was simply composed of a normal 2-D projector and a screen without using extra optics. In our binocular system, reflected light rays converged to the left and right eyes of the observer and the crosstalk was less than 8%. In the light field system, the reflected light rays formed a spatially sampled light field and focused a virtual object in a depth range of ± 30 mm with a ± 13.5 -deg viewing angle. By developing wavefront printing technology, a complex optics array may easily be printed by nonprofessionals for optics manufacturing. © The Authors. Published by SPIE under a Creative Commons Attribution 3.0 Unported License. Distribution or reproduction of this work in whole or in part requires full attribution of the original publication, including its DOI. [DOI: [10.1117/1.OE.57.6.061605](https://doi.org/10.1117/1.OE.57.6.061605)]

Keywords: wavefront printer; hologram printer; holographic optical element; binocular display; light field display; holography.

Paper 171740SSP received Oct. 31, 2017; accepted for publication Dec. 29, 2017; published online Jan. 27, 2018; corrected Apr. 18, 2018.

1 Introduction

Static hologram printing services have been commercialized^{1–3} for more than a decade. Also, compact desktop full-color printers⁴ have recently been proposed. These printers basically use holographic stereograms (HS). Unlike an HS printer, fringe printers and wavefront printers^{5–9} can theoretically record a hologram that reconstructs a very sharp point light source (3-D object point) that is located far from the hologram. In contrast to an HS printer, a wavefront printer records an arbitrary wavefront with full control of both the amplitude and phase distribution reconstructed by a computer-generated hologram¹⁰ (CGH) displayed on a spatial light modulator (SLM). The number of pixels in a conventional SLM is insufficient to record a large hologram in a single shot; thus, computer-controlled *X-Y* linear stages are normally used and the entire hologram is divided into many subholograms.

A hologram generated by a wavefront printer is useful for static 3-D scene visualization applications^{11,12} due to its ability to reproduce the deep focusing range of a 3-D point. However, it is also expected to be useful for fabricating large complex optical elements, such as microsize nonspherical lens arrays, anamorphic lens arrays, and multiple focal-length lens arrays,¹³ used in precisely designed 3-D displays. An appropriate subhologram size is one of the important factors that ensure the quality of resulting images. In this paper, we describe our wavefront printer, which uses a photopolymer as a holographic material, and discuss the subhologram size. Furthermore, we discuss two examples of reflective 3-D screens fabricated using the printer. In these screens, optical

cells (subholograms) are formed by the numerical calculation of holograms, and they are also features of a different optical axis depending on the cell position.

2 Holographic Wavefront Printer

This section describes the optical settings of our hologram printer and the 3-D data printing method using the printer. Applications of static holograms are also described.

2.1 Wavefront Printer

Recently, Bruder et al.¹⁴ have reported a large diffractive optical element, in which the divided wavefront of the designed optical function is reconstructed using a phase SLM and a large transparent-type holographic optical element (HOE) is stitched by writing many slightly different small HOEs. We also employ basically the same procedure to form reflective-type holograms and HOEs using an amplitude SLM with 4K resolution, as shown in Fig. 1. Bruder et al. claimed that a Fourier lens is needed to generate the phase function in a hologram printer using an amplitude SLM. However, we did not use a Fourier lens but electronic holography^{15–17} technique to generate an arbitrary phase distribution. The optical system of our wavefront printer uses a collimated laser beam with 532-nm wavelength. First, the beam is split by a polarization beam splitter. The two beams are used as an object beam and a reference beam to record a subhologram as a reflection-type volume hologram. The object beam is modulated as a part of the entire wavefront on the hologram using subhologram data displayed on an SLM (JVC Kenwood Corporation D-ILA[®] 4K2K LCOS). Undesirable lights, i.e., the transmission beam, high-order beam, and conjugate beam, are filtered out by a single-side band filter and a half-zone plate processing

*Address all correspondence to: Ryutaro Oi, E-mail: oi.ryutaro@nict.go.jp

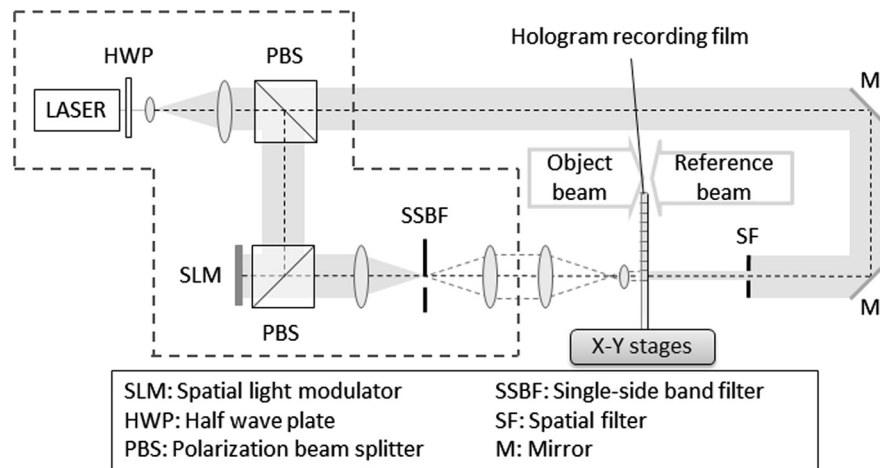


Fig. 1 Schematic of hologram printer.

method¹⁷⁻¹⁹ similar to an electronic holography system.¹⁵⁻¹⁷ Then, the optical system demagnifies the modulated wavefront onto a holographic recording film made of covestro Bayfol[®] HX102 photopolymer material. The reference beam is a plane wave and is incident perpendicular to the photopolymer from the opposite side of the object beam. Table 1 shows the specifications of the wavefront printer. Because the resolution of the motorized X-Y stage (Chuo

Table 1 Parameters of the wavefront printer.

Wavelength	532 nm
Subhologram resolution	up to 3800 × 2100
SLM resolution	3840 × 2160
SLM pixel pitch	3.5 μm, 4.8 μm (depending on the SLM)
Magnification ratio	1:0.1, 1:0.077 (depending on the SLM)
X-Y positioning accuracy	less than 4.0 μm
Recording material	Covestro Bayfol [®] HX102

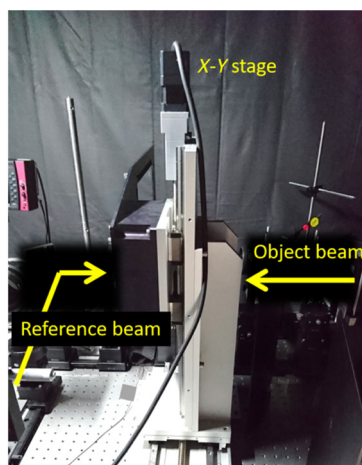


Fig. 2 Experimental setup of holographic wavefront printer.

Precision Industrial ALZ-230-C2P) is ~4.0 μm, wavefronts will, in practice, be disconnected at the edge of each subhologram (Fig. 2). After recording of all the subholograms, the holographic recording material is then processed by bleaching²⁰ to obtain higher transmittance at visible-light wavelengths.

2.2 Overlap Print for Better 3-D Scene Reconstruction

The dividing process in the hologram recording causes phase discontinuity between the subholograms (cells), and the reconstructed holographic image also has severe split lines and phase discontinuity, as shown in Fig. 3(a), which shows a reconstructed image with 648-μm cell size and 648-μm cell pitch printed using our printer.²¹ One possible solution to this problem is to use a subhologram size smaller than the spatial resolution of the observer's eyesight. In the case of static hologram application, the cell size should be less than 87 μm when the hologram is observed at a distance of 30 cm and the resolution of the observer eyesight is 1 deg/60. However, the phase discontinuity at the neighboring subholograms also causes image degradation due to the diffraction effect, particularly when the subhologram is too small. From the viewpoint of diffraction, the cell size should be large unless 3-D objects or scenes are placed very close to the hologram.^{11,21} The wavefront reconstructed by one subhologram is considered to be the same as that reproduced by a hologram with a finite square aperture. When the subhologram width is D , the finite aperture $P(x)$ on the x -axis is expressed by

$$P(x) = \prod\left(\frac{x}{D}\right) = \begin{cases} 1 & |x| \leq \frac{D}{2} \\ 0 & |x| > \frac{D}{2} \end{cases} \quad (1)$$

When the distance between the hologram and a point light source is d and the wavefront of the point light source is recorded on the hologram, the wavefront reconstructed by the subhologram is the convolution of the entire hologram and the finite aperture. The Fourier transform of the finite aperture is expressed as

$$\bar{P}(f_x) = \mathcal{F}\{P(x)\}_{f_x = \frac{x_i}{\lambda d}} = D \operatorname{sinc}\left(D \frac{x_i}{\lambda d}\right), \quad (2)$$

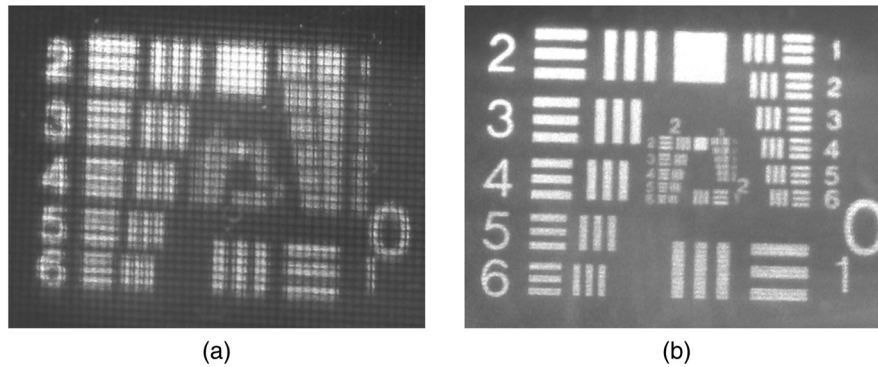


Fig. 3 Magnified overlapped and nonoverlapped images printed using the wavefront printer: (a) 648- μm nonoverlap image and (b) 648- μm image printed with 324- μm overlap.

where λ is the wavelength of the light source. The resolution of the point light source depends on the width of the main lobe of the sinc function. The sinc function vanishes when $D \times f_x$ is $\pm 1, \pm 2, \pm 3, \dots$; thus, the resolution Δx_i is expressed by the following equation:

$$\Delta x_i = \frac{2\lambda d}{D}. \quad (3)$$

The resolution Δy_i along the x -axis can be expressed in the same manner. For example, when $\lambda = 532 \text{ nm}$, $D = 87 \mu\text{m}$, and $d = 50 \text{ mm}$, then Δx_i is $611 \mu\text{m}$, which is seven times larger than the subhologram size, and the resulting 3-D image may be blurred.

Overlap printing is one solution to this contradicting cell-size problem. Since the photopolymer can record multiple wavefronts in one subhologram, by using a larger cell size D and shifting each subhologram by $D/2$ in vertically and horizontally, a large aperture size and small cell size can be simultaneously achieved while concealing the dark areas of split lines. Figure 3(b) shows an image reconstructed by overlapping 648- μm subholograms with a 324- μm shift.

2.3 Real/Virtual 3-D Data Visualization Applications

Three-dimensional data of both real and virtual objects were recorded using our wavefront printer. CGHs of a real object, a miniature Buddha statue, and a virtual object, computer graphics (CG) data of Venus, were calculated on the ray-sampling plane by a fast calculation method. Perspective images with a number of 544×544 viewpoints were rendered for each hologram using conventional CG software and each view had 512×512 resolution. The resulting hologram had the same number of pixels as the input perspective images, $278,528 \times 278,528$ pixels in total. For the real object, 47 images from different viewpoints were taken using a handheld camera, which were combined by Autodesk® 123D Catch²² to form a solid 3-D object. The conversion from the 47 2-D pictures to the 3-D object was fully automated and the data were transferred to conventional CG software.

The generated hologram was divided into 155×155 subholograms because we used a cell size of 3600×1800 pixels in the wavefront printer in this experiment. Figures 4(a) and 4(c) show the input 3-D data of Venus and Buddha. Figures 4(b) and 4(d) show the optical reconstruction from printed holograms, respectively. Both the virtual and real

objects were successfully reconstructed from the holograms. Since the recorded holograms have the wavelength selectivity inherent to reflection-type volume holograms, white-light illumination was used in this experiment.

3 Reflection 3-D Screen and Application

In this section, projection 3-D video displays employing a digitally designed HOE (DDHOE) are introduced. The DDHOE was fabricated using the wavefront printer and has several advantages over conventional volume-type HOE,^{23–27} which are shaped by an analog hologram recording procedure. Since a DDHOE is recorded by stitching many small optical cells, it can easily provide a microscale optical element array without any additional cost. It can also provide complex optical functions, such as a multiple focal-length lens array¹³ printed using numerical data because an SLM can ideally reproduce any complex amplitude. It can also be used to compose nonspherical lens array without using real existing optics before the DDHOE is manufactured.

3.1 Transparent Glasses-Free Binocular Display

Some glasses-free 3-D displays are now commercially available^{28,29} but 3-D glasses are more commonly used. Some advantages of 3-D glasses are their low crosstalk, the 2-D/3-D compatibility of the video screen, and the low cost.

In glasses-free 3-D displays, a lenticular lens array or a parallax barrier array is often used^{30,31} to converge light emitted from the screen to the L/R eye positions of the human observer. A major disadvantage of these arrays is that the resolution may be reduced along the horizontal axis.³⁰ Visual artifacts including view reversals³⁰ as well as the visibility of the light-guiding array components³¹ are also problems.

Here, we consider a binocular 3-D display application of the DDHOE.^{32,33} Figure 5 shows our experimental setup of the glasses-free system. The system consists of a 2-D projector and a DDHOE screen that was printed using the hologram printer. The projector (Sanwa Supply 400-PRJ021, resolution of 1280×720) was used without any modification (the focusing distance was set to $\sim 520 \text{ mm}$ by adjusting the focusing dial). The left image is projected on odd lines on the screen and right image is projected on even lines. The DDHOE was designed to selectively reflect even lines to the right eye of humans. The observation distance was set to 700 mm from the screen.



Fig. 4 Virtual scene and real object converted into hologram and printed by hologram printer: (a) virtual objects, (b) printed hologram of virtual objects, (c) real object, and (d) printed hologram of real object.



Fig. 5 Experimental setup of glasses-free binocular 3-D display.

3.1.1 Spherical wave from the projector

The size of the screen was chosen to be 100 mm × 100 mm. As shown in Fig. 6(a), the incident angle of the ray at the top edge of the screen is 10.9 deg to the normal vector, whereas the angle at the bottom edge of the screen is 0 because the projector has a diverging angle in the vertical direction. The DDHOE is designed to converge whole light rays toward the observer's eye height (271 mm), as shown in Fig. 6(b).

The horizontal reflection function was designed in the same manner as the above-mentioned vertical function. The incident light from the projector is a spherical wave (radius of 520 mm), and the incident angle at the side edges was calculated to be 5.5 deg to the normal vector, as shown in Fig. 7(a). Figure 7(b) shows the reflection from even lines of the DDHOE. All the reflected rays converge at the right eye position, which is 31 mm from the center of the projector.

3.1.2 Printing the DDHOE

The screen used for the binocular display consists of many planar micromirrors with a dedicated tilt angle to the optical axis. These micromirrors were printed by the interference between two planewaves inside the wavefront hologram printer. A plane wave with an arbitrary incident angle was generated accordingly using the Lohmann CGH technique.¹⁰ Complex amplitude of a plane wave $\mathbf{P}_{1(x,y)}$ with an incident angle of θ to the x -axis and incident angle of φ to the y -axis is expressed by

$$\mathbf{P}_{1(x,y)} = e^{-i\frac{2\pi}{\lambda}(x \cdot \sin \theta + y \cdot \sin \varphi)}, \quad (4)$$

where λ is the wavelength. The reference beam $\mathbf{R}_{1(x,y)}$ is written using the following equation:

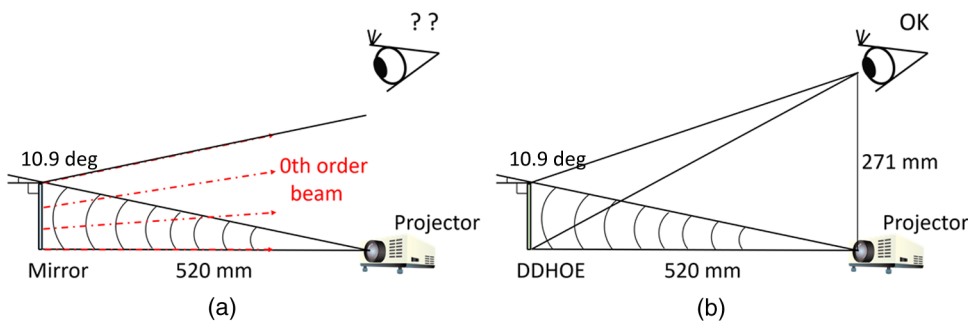


Fig. 6 Side view of glasses-free binocular display: (a) with mirror and (b) with DDHOE.

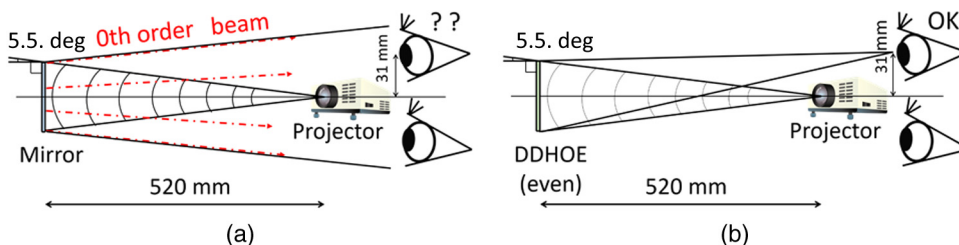


Fig. 7 Top view of glasses-free binocular display: (a) with mirror and (b) with DDHOE.

Table 2 Specification of glasses-free binocular screen.

Number of micromirrors	93 (h) × 187 (v)
HOE screen size	96.34 mm (h) × 96.8 mm (v)
Tilt angle of mirrors (horizontal)	−11.7 deg to +11.7 deg (depending on the location)
Tilt angle of mirrors (vertical)	+21.1 deg to +10.5 deg (depending on the location)
Projection distance	520 mm
Viewing distance	700 mm
Viewing height	271 mm
Micromirror size	1.036 mm (h) × 0.518 mm (v)
Width of each odd/even line	2.072 mm
Design wavelength	532 nm
HOE material	Bayfol® HX102

$$\mathbf{R}_{1(x,y)} = e^{i\frac{2\pi}{\lambda}[x \cdot \sin(\theta) + y \cdot \sin(\varphi)]} \quad (5)$$

The amplitude hologram $I_{1(x,y)}$, which is displayed on the SLM, is written as the square of the complex sum of the object beam $\mathbf{P}_{1(x,y)}$ and the reference beam $\mathbf{R}_{1(x,y)}$ and expressed by

$$I_{1(x,y)} = |\mathbf{P}_1 + \mathbf{R}_1|^2 = 2 \cdot \cos\left\{\frac{2\pi}{\lambda}(x \cdot \sin \theta + y \cdot \sin \varphi)\right\} + |\mathbf{P}_1|^2 + |\mathbf{R}_1|^2. \quad (6)$$

Hologram $I_{1(x,y)}$ is numerically calculated using a computer with a 32-bit floating-point number (approximately seven-digit accuracy) then rounded off to an 8-bit unsigned integer to be displayed on the SLM. Table 2 shows the specifications of the prototype DDHOE screen.

3.1.3 Binocular 3-D display

The prototype binocular screen was glued to a glass substrate (1.0 mm thickness) and placed at a distance of 500 mm from the projection lens. Figures 8(a)–8(c) depict the reflection function of the prototype DDHOE. Figure 8(a) is a photograph taken in a dark room using a smoke machine (Antari Z-800 II); the projector displays a solid green square on the screen. Incident light from the projector to the screen has a diverging angle and the reflected light converges to the

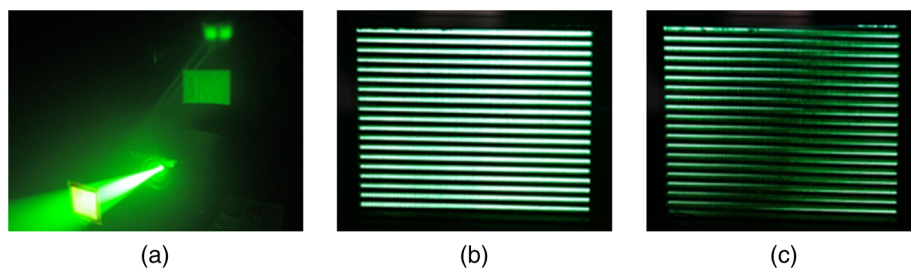


Fig. 8 Reflection function of the printed DDHOE: (a) light converges at eyes, (b) from left eye, and (c) from right eye.

positions of two human eyes. The bright square area just below the converged light is a direct reflection at the DDHOE glass substrate (zeroth-order beam), and this component appears a different position from the first-order diffracted beam. The images in Figs. 8(b) and 8(c) show the results of examining crosstalk. A horizontal strip pattern consisting of only odd lines is projected onto the DDHOE. According to the design, only the left image should be bright. A bright strip is visible in Fig. 8(b), which was from the left-eye position, whereas it is invisible in Fig. 8(c), which was taken from the right-eye position. The opposite result was obtained when a strip pattern consisting of even lines was projected on the screen (images not shown). The crosstalk light components were measured by a lux meter (Konica Minolta® CL-200A) and the maximum leakage power was 8% for both the R image to the left and the L image to the right eye.

Figures 9(a)–9(d) show the result of optical reconstruction. The images in Figs. 9(a) and 9(c) were taken using a digital camera from the left-eye position, and those in Figs. 9(b) and 9(d) were taken from the right-eye position. The observed left-eye image and right-eye image had the designed disparity, as shown in Figs. 9(c) and 9(d); thus, the 3-D virtual image could be seen without using glasses. Since the DDHOE screen has wavelength selectivity in accordance with the principle of volume holograms, the screen can be used for white-light illumination from a projector. The DDHOE screen also has high transmittance for visible light (400 to 760 nm), allowing background objects to be seen through the prototype screen, as shown in Fig. 10.

3.2 Diffraction Light Field Display

Light field displays have the ability to induce the accommodation of human eyes as well as motion parallax. Since Lippmann first reported³⁴ a static integral photography display, many light field video displays have been proposed.^{34–39} In these displays, numerous elemental images are arranged vertically and horizontally, and a microlens array (MLA) is used to control the directions of light rays

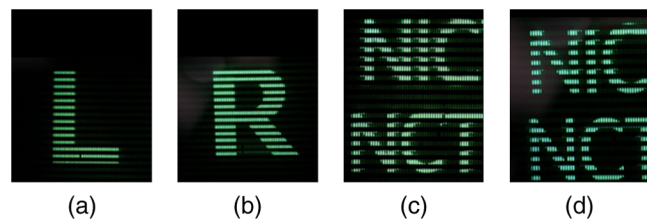


Fig. 9 Optical reconstruction of binocular display: (a) from left, (b) from right, (c) from left, and (d) from right.

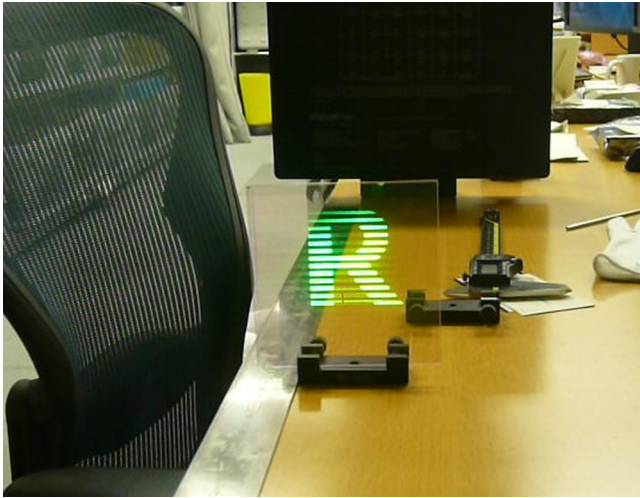


Fig. 10 Example video of the binocular display (Video 1, MOV, 72.5 MB [URL: <http://dx.doi.org/10.1117/1.OE.57.6.061605.1>]).

emitted from the screen. Although some MLAs are commercially available, custom-made MLAs are very costly because of the complex manufacturing process.

Light field screens made from an analog HOE (instead of an MLA) have been proposed and a 2-D/3-D switchable function,⁴⁰ different spatial multiplexing optical functions,²⁵ and other applications of the HOE have been reported. However, in the previous research, the HOEs were fabricated by copying a phase distribution generated by real existing optics, such as MLAs, objective lenses, or optical diffusers.

Here, we propose a light field screen made from a DDHOE. Since a DDHOE is fabricated by recording a numerically generated phase distribution without using any optical molds, complex optical functions for the light field screen can be easily realized by nonprofessionals for using optical hardware.

The system consists of a 2-D projector and a DDHOE light field screen, as shown in Fig. 11(a). A 4K projector (Sony® VPL-VW515, 3840 × 2160 resolution.) was used because the light field system⁴¹ requires more pixels than the former binocular system. The screen is a reflection-type light field screen, thus, basically, consists of arbitrarily tilted concave micromirrors. The DDHOE was designed to compensate the spherical wave from the projector to a parallel wave for the same reason, as described in

Sec. 3.1.1. Figure 11(b) shows the fabricated light field screen. The projection distance was set to 567.5 mm in accordance with the diverging angle of the projector and the height of the DDHOE screen. The observation distance was not set in this system; thus, the principal rays reflected by the elemental mirrors exited at an angle of 9.8 deg to the normal vector of the screen.

3.2.1 Fabrication of light field DDHOE screen

The prototype DDHOE screen is composed of numerous tilted mirrors. The phase modulation $P_{2(x,y)}$ of a concave mirror, whose focal length is f (mm), can be written as follows:

$$P_{2(x,y)} = e^{-ik \frac{x^2+y^2}{2f}}, \quad (7)$$

where k is the wave number. The tilt angle (θ, φ) of the mirror can be described by Eq. (4). The reference beam in the wavefront printer is always incident normal to the SLM; thus, the complex amplitude of the reference beam can be written as Eq. (5). In total, an amplitude hologram $I_{2(x,y)}$ that reconstructs a tilted concave mirror function is written as follows:

$$I_{2(x,y)} = 2 \cdot \cos \left\{ k \cdot \left(\frac{x^2 + y^2}{2 \cdot f} + x \cdot \sin \theta + y \cdot \sin \varphi \right) \right\}. \quad (8)$$

The hologram calculation was performed on Visual Studio® C++ 2012, and the resulting amplitude holograms were stored in an HDD as bitmap data. Each bitmap was retrieved and displayed on the SLM to modulate the illumination beam from the laser (Cobolt Samba™ 100 mW at 532 nm) in the printer. In the printing of prototype DDHOE, an SLM with a center area of 2800 × 1400 pixels was used to generate the object beam. The printing time for one 100 × 100 mm DDHOE was ~16 h. The waiting time to reduce the vibration of the printer hardware accounts for more than 60% of the total printing time (2.0 s in each cell). An active vibration-cancelling system would help to solve this problem. Reducing the exposure time through the use of a more powerful laser may be another means of reducing the long printing time. The resulting DDHOE parameters used for the light field display are shown in Table 3.

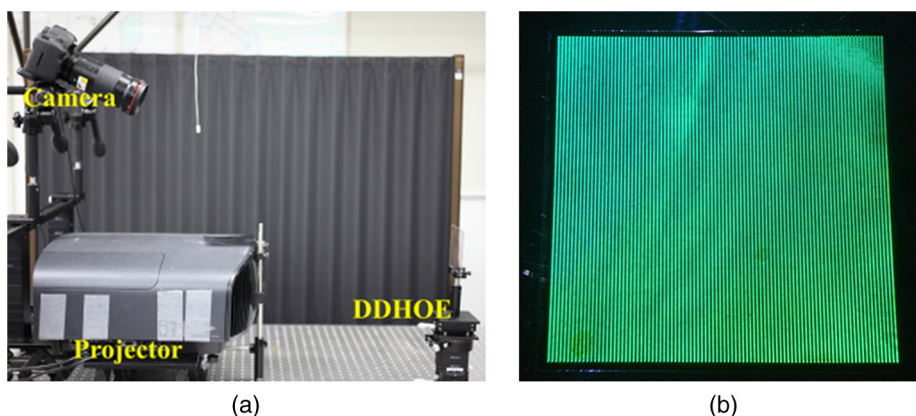


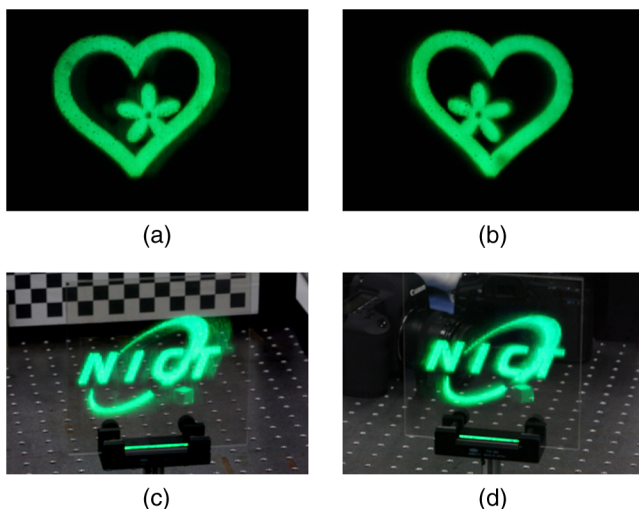
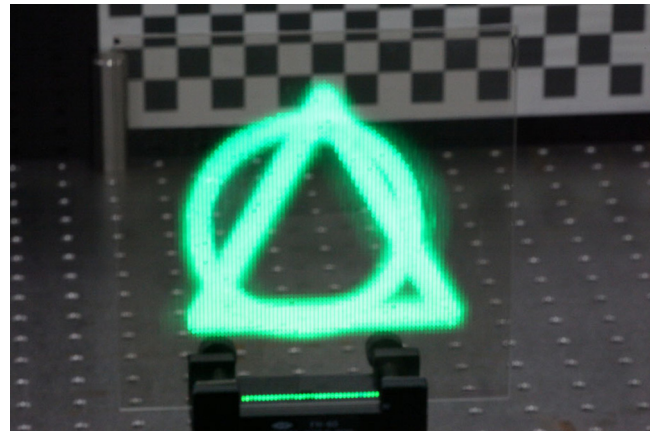
Fig. 11 Light field display using DDHOE screen: (a) experimental setup and (b) prototype light field screen.

Table 3 Specification of light field screen.

Number of concave mirrors	93 (h) × 187 (v)
HOE screen size	96.34 mm (h) × 96.8 mm (v)
Tilt angle of concave mirrors (horizontal)	−4.85 deg to +4.85 deg (depending on location)
Tilt angle of concave mirrors (vertical)	+0.3 deg to +9.80 deg (depending on location)
Focal length of concave mirror	2.16 mm
Viewing angle	±13.5 deg (h), +13.5 deg to 0 deg (v)
Viewing distance	0 mm to ∞
Concave micromirror size	1.036 mm (h) × 0.518 mm (v)
Design wavelength	532 nm
HOE type	Reflective volume HOE

3.2.2 Light field display

The prototype light field screen was fixed in front of a 2-D projector at a distance of 567.5 mm. CG software (Blender 2.76) was used for rendering virtual 3-D objects to form 17,391 elemental images. Figures 12(a)–12(d) show reconstructed light field images taken by a digital camera from different positions. To obtain Figs. 12(a) and 12(b), a heart-shaped object was placed 25 mm behind the screen, and a flower pattern was placed 25 mm in front of the screen. Motion parallax can be clearly observed in these images. When a virtual object was placed farther than 30 mm from the screen, the reconstructed image gradually became blurred. Figures 12(c) and 12(d) also show “logo” contents taken by a digital camera (Canon[®] EOS-5DMK2, 180 mm, F3.5). An ellipse was placed 25 mm behind the screen and letters were placed 25 mm in front of the screen. The viewing angle of the light field display was ~27 deg, which is equivalent to the designed parameter. The prototype screen has wavelength selectivity and the green component of the


Fig. 12 Reconstructed 3-D images using the DDHOE light field screen.

Fig. 13 Example video of the light field display (Video 2, MP4, 6.6 MB [URL: <http://dx.doi.org/10.1117/1.OE.57.6.061605.2>]).

projected light is visible from the observer, as shown in Fig. 13. The viewing angle of our system is restricted owing to the limited range of the diffraction angle in our wavefront hologram printer. The direct reflection of the projector light from the screen is slightly below the first-order diffracted light component; thus, it does not hinder the reconstructed light field image.

4 Conclusion

In this paper, a wavefront printer that records reflective volume holograms and several of its applications were described. The overlap printing technique used in our wavefront printer can effectively conceal the stitch lines between subholograms. The generation of large holograms for visualizing static 3-D scene is the most promising application of the printer while it is also useful for fabricating optical screens with relatively complex optical functions determined by numerical calculation. A 10-cm prototype glasses-free binocular display and a prototype light field display with a viewing angle of 27 deg were reported in this paper. In both prototypes, we used a commercially available 2-D projector and a screen that was printed using our wavefront printer, and the expected 3-D images were observed. Because of a hardware limitation of our printer, experiments were undertaken at a wavelength of 532 nm. The fabrication of full-color-capable HOEs will be considered in future.

Acknowledgments

This research was supported by Japan Society for the Promotion of Science (JSPS) KAKENHI; Award Nos. JP16H01742 and JP26790064. The part of this research and development was supported by MIC/SCOPE; Award No. 162103005.

References

1. Geola, “Lasers holograms photomaterials,” <http://geola.com/> (27 December 2017).
2. Holotech, “Satellite 3D imaging,” <http://holotech3d.com/> (27 December 2017).
3. Holoxica, “Static Digital Holograms,” <http://www.holoxica.com/technology/> (27 December 2017).
4. Y. Ito et al., *Development of Full-Color Hologram Printer*, pp. 1–7, Pioneer R&D, Tokyo, Japan (2014).
5. T. Yamaguchi, O. Miyamoto, and H. Yoshikawa, “Volume hologram printer to record the wavefront of three-dimensional objects,” *Opt. Eng.* **51**(7), 075802 (2012).

6. W. Nishi and K. Matsushima, "A wavefront printer using phase-only spatial light modulator for producing computer-generated volume holograms," *Proc. SPIE* **9006**, 90061F (2014).
7. Y. Kim et al., "Seamless full color holographic printing method based on spatial partitioning of SLM," *Opt. Express* **23**(1), 172 (2015).
8. H. Kang et al., "Color wavefront printer with mosaic delivery of primary colors," *Opt. Commun.* **350**, 47–55 (2015).
9. H. Kang et al., "Color holographic wave-front printing technique," in *IEEE 13th Int. Conf. on Industrial Informatics (INDIN '15)*, p. 686 (2015).
10. A. W. Lohmann and D. P. Paris, "Binary Fraunhofer holograms generated by a computer," *Appl. Opt.* **6**(10), 1739–1748 (1967).
11. K. Wakunami et al., "Wavefront printing technique with overlapping approach toward high definition holographic image reconstruction," *Proc. SPIE* **9867**, 98670J (2016).
12. K. Wakunami et al., "Projection-type see-through holographic three-dimensional display," *Nat. Commun.* **7**, 12954 (2016).
13. S. W. Min, B. Javidi, and B. Lee, "Enhanced three-dimensional integral imaging system by use of double display devices," *Appl. Opt.* **42**(20), 4186–4195 (2003).
14. F.-K. Bruder et al., "Diffraction optics in large sizes: computer-generated holograms (CGH) based on Bayfol HX photopolymer," *Proc. SPIE* **9385**, 93850C (2015).
15. T. Mishina, M. Okui, and F. Okano, "Viewing-zone enlargement method for sampled hologram that uses high-order diffraction," *Appl. Opt.* **41**(8), 1489–1499 (2002).
16. H. Sasaki et al., "Large size three-dimensional video by electronic holography using multiple spatial light modulators," *Sci. Rep.* **4**, 6177 (2014).
17. T. Mishina, F. Okano, and I. Yuyama, "Time-alternating method based on single-sideband holography with half-zone-plate processing for the enlargement of viewing zones," *Appl. Opt.* **38**(17), 3703–3713 (1999).
18. O. Bryngdahl and A. Lohmann, "Single-sideband holography," *J. Opt. Soc. Am.* **58**(5), 620–624 (1968).
19. T. Takemori, "3-dimensional display using liquid crystal devices—fast computation of hologram," The Institute of Image Information and Television Engineers (ITE) Technical Report 21, pp. 13–19, Tokyo, Japan (1997).
20. H. Berneth et al., "Byfor HX photopolymer for full-color transmission volume Bragg gratings," *Proc. SPIE* **9006**, 900602 (2014).
21. Y. Ichihashi et al., "An analysis of printing conditions for wavefront overlapping printing," *Proc. SPIE* **10127**, 101270L (2017).
22. Autodesk, "123D," <https://www.autodesk.com/solutions/123d-apps/> (27 December 2017).
23. K. Hong et al., "Full-color lens-array holographic optical element for three-dimensional optical see-through augmented reality," *Opt. Lett.* **39**(1), 127–130 (2014).
24. M. Yamaguchi, "Light-field and holographic three-dimensional displays," *J. Opt. Soc. Am.* **33**(12), 2348–2364 (2016).
25. C. Jang et al., "See-through integral imaging displays using a resolution and fill factor-enhanced lens-array holographic optical element," *Opt. Exp.* **22**(23), 27958–27967 (2014).
26. R. Higashida and M. Yamaguchi, "Automatic geometric calibration in full-parallax 3D display using holographic screen," in *Institute of Image Information and Television Engineers Annual convention*, pp. 1–2 (2014).
27. C. Jang et al., "Recent progress in see-through three-dimensional displays using holographic optical elements," *Appl. Opt.* **55**(3), A71–A85 (2016).
28. Fujifilm, "FinePix® REAL 3D W3," http://www.fujifilm.com/products/3d/camera/finepix_real3dw3/ (27 December 2017).
29. Nintendo, "NINTENDO 3DS™," <https://www.nintendo.com/3ds/> (27 December 2017).
30. S. E. Brigham and J. Schultz, "Directional backlight timing requirements for full resolution autostereoscopic 3D Displays," in *Proc. SID Symp. Digest of Technical Papers*, Vol. 41, pp. 226–229 (2010).
31. U. Vogel et al., "OLED backlight for autostereoscopic displays," *Proc. SPIE* **7237**, 72730U (2009).
32. R. Oi et al., "Glassless 3D screen using HOE for spherical wave compensation," in *17th Int. Meeting on Information Display and 9th Int. Conf. on 3D Systems and Applications (3DSA '17)*, Busan, South Korea (2017).
33. P.-Y. Chou et al., "A calibrating method for projected-type auto-stereoscopic 3D display system with DDHOE," in *Int. Display Manufacturing Conf. 2017 (IDMC'17)*, Taipei, Taiwan (2017).
34. M. G. Lippmann, "Épreuves réversibles donnant la sensation du relief," *J. Phys. Theor. Appl.* **7**(1), 821–825 (1908).
35. T. Okoshi, *Three-Dimensional Imaging Techniques*, Academic Press, Tokyo, Japan (1976).
36. F. Okano et al., "Real-time pickup method for a three-dimensional image based on integral photography," *Appl. Opt.* **36**(7), 1598–1603 (1997).
37. J. Y. Son et al., "Three-dimensional imaging for creating real-world-like environments," *Proc. IEEE* **101**(1), 190–205 (2013).
38. J.-S. Jang and B. Javidi, "Three-dimensional projection integral imaging using micro-convex-mirror arrays," *Opt. Exp.* **12**(6), 1077–1083 (2004).
39. J. Arai et al., "Integral three-dimensional television with video system using pixel-offset method," *Opt. Exp.* **21**(3), 3474–3485 (2013).
40. J. Yeom et al., "Three-dimensional/two-dimensional convertible projection screen using see-through integral imaging based on holographic optical element," *Appl. Opt.* **54**(30), 8856–8862 (2015).
41. B. J. Jackin et al., "Calibration and quality improvement of projection type Integral 3D display," in *17th Int. Meeting on Information Display and 9th Int. Conf. on 3D Systems and Applications (3DSA '17)*, Busan, South Korea (2017).

Ryutaro Oi is a senior researcher at Electromagnetic Applications Laboratory, Applied Electromagnetic Research Institute, National Institute of Information and Communications Technology (NICT), Japan. He received his PhD degree in science from the University of Tokyo in 2004. He was a visiting researcher at Japan Broadcasting Corporation (NHK) Science and Technology Research Laboratories in 2004 and 2005. He joined NICT as a researcher in 2006. His areas of interests include holography and autostereoscopic 3-D displays.

Ping-Yen Chou received his BS and MS degrees in photonics engineering from National Chiao Tung University, Hsinchu, Taiwan, in 2011 and 2012, respectively. During his master's degree, he conducted a project with Sony Corporation, Tokyo, Japan, and published in the Society for Information Display, International Conference 2012. Currently, he is a fourth-year PhD student in the Institute of Electro-Optical Engineering at NCTU and has conducted research about 3-D image display systems and integral photography theory.

Boaz Jessie Jackin received his PhD degree from the Center for Optical Research and Education, Utsunomiya University, in 2013 and then continued as a postdoc researcher in the same university until 2016. Since 2016, he has worked as a researcher at the National Institute of Information and Communications Technology (NICT) in Japan. His current research interest includes computer-generated holography, digital holography, and light field display.

Koki Wakunami is a senior researcher at Electromagnetic Applications Laboratory, Applied Electromagnetic Research Institute, National Institute of Information and Communications Technology (NICT) Japan. He received his DrEng degree from Tokyo Institute of Technology in 2013. His current research interests include computational holography and electronic holography system.

Yasuyuki Ichihashi is a senior researcher at the National Institute of Information and Communications Technology (NICT), Japan. He received MsEng and PhD degrees in 2007 and 2010 from the Chiba University in Japan. He was on loan to the Council for Science, Technology and Innovation of the Cabinet Office in 2015. His research area is calculating method of hologram for wavefront printer and evaluating 3-D images and holographic optical element reconstructed from the holograms.

Makoto Okui received his BS, ME, and DE degrees from Tokyo Institute of Technology, Tokyo, Japan, in 1978, 1980, and 2006, respectively. He joined NHK (Japan broadcasting Corporation) in 1980. He conducted research and development on television technology including three-dimensional television at NHK STRL from 1983 to 2013. He is currently a senior researcher of the Electromagnetic Applications Laboratory at the National Institute of Information and Communications Technology (NICT) of Japan.

Yi-Pai Huang is currently a professor at National Chiao-Tung University. His expertise includes visual science, 3-D technology, and display optics. He has published 65 journal papers, 150 international conference papers, 93 patents, and 3 book chapters. He was awarded the Google research award and SID Peter Brody Prize in 2017; four times received the SID's distinguished paper award (2001, 2004, 2009, 2015), and two times of SPIE Fumio Okano Best 3-D paper prize.

Kenji Yamamoto received his PhD degree from Nagoya University. He is a chief senior researcher at NICT. His research interests include 3-D visual system and HOE, especially wavefront printer, computer-generated hologram, integral photography, and multiview video coding. He serves as a vice president in holographic display artists and engineers club (HODIC) under OSJ, executive director in ultra-realistic communications forum (URCF), program chair in 3DSA, program chair of 3-D workshop in IDW, chair of AR/VR subcommittee in SID Japan chapter, etc.